Geoderma 437 (2023) 116576

Contents lists available at ScienceDirect

Geoderma

journal homepage: www.elsevier.com/locate/geoderma

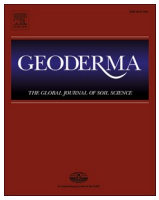

Variations in pore size and contact angle distributions control rhizosphere rewetting

P. Benard [a,*], J. Bachmann [b], M. Zarebanadkouki [c], S. Schlüter [d], S.R.G.A. Blaser [d], A. Kaestner [e], A. Carminati [a]

[a] Physics of Soils and Terrestrial Ecosystems, Department of Environmental Systems Science, ETH Zurich, Universitätsstrasse 16, Zürich 8092, Switzerland
[b] Institute of Soil Science, Department of Environmental Sciences, University of Hannover, Herrenhäuser Straße 2, Hanover 30419, Germany
[c] Soil Biophysics and Environmental Systems, Department of Life Science Systems, Technical University of Munich, Alte Akademie 8, Freising 85354, Germany
[d] Department of Soil System Science, Helmholtz Centre for Environmental Research – UFZ, Theodor-Lieser-Str. 4, Halle 06120, Germany
[e] Paul Scherrer Institute, Laboratory for Neutron Scattering and Imaging, Forschungsstrasse 111, Villigen 5232, Switzerland

ARTICLE INFO

Handling Editor: Yvan Capowiez

Keywords:
Soil wettability
Rhizosphere
Mucilage
Neutron imaging
Pore network model

ABSTRACT

Rhizosphere wettability decreases upon severe drying leading to periods of prolonged low water content around roots after precipitation or irrigation. These observations were explained by the temporal hydrophobic character of mucilage, while structural alterations of the pore space caused by mucilage, such as pore clogging, remained mostly unexplored. In this study, time-series neutron radiography and a pore network model were used to assess the impact of pore geometry and wettability on water flow following the addition of mucilage in a sand substrate. To do so, we monitored the capillary rise of ethanol and water separately for mucilage contents, ranging from 0.0 to 2.0 mg g^{-1}. A pore network model was developed to analyze the impact of alterations in pore geometry and wettability. Results are compared with analytical solutions of the Lucas-Washburn equation. Rewetting dynamics were explained by a combination of a decrease in effective pore throat size and a global decrease in wettability. The local distribution of wettability, however, appeared of minor importance as dynamics of water imbibition could be matched by a uniform effective contact angle. For 0.1 mg g^{-1} mucilage content increased wettability was predicted for both approaches: the analytical solution and the pore network model fit. At larger contents, a decrease in wettability occurred which was accompanied by a decrease in derived effective pore and pore throat size. On a minute scale, rewetting appeared to steadily progress at all mucilage contents with accelerated rewetting observed at 0.6 mg g^{-1} likely related to an increased wetting front length. This study highlights the importance of mucilage on pore geometry in combination with wettability modifications in the rhizosphere. Aside from rhizosphere rewetting, the presented approach provides an opportunity to investigate further wettability-related processes in other soil environments on various spatial scales.

1. Introduction

The rhizosphere comprises the volume of soil actively modified by root growth and exudation with its physical and chemical properties being distinct from its surrounding bulk soil (Gregory, 2006). As an estimated 40% of all terrestrial precipitation flows through this thin region (Bengough, 2012), it is vital to understand the basic principles of modifications induced by root exudation (Hallett et al., 2022). In addition to various sugars, amino and organic acids, which are known to promote microbial activity in the rhizosphere (Kuzyakov and Blagodatskaya, 2015), mucilage with significant impact on physical processes is also released into the rhizosphere (Roberts, 1916; Oades, 1978). Consisting of a blend of extracellular polymeric substances (EPS), mucilage shares many of its features with other highly polymeric compounds found in nature, like bacterial EPS in biofilm (Benard et al., 2019). In the rhizosphere, many of the water related alterations observed within this soil volume of a few millimeters in thickness around roots (Holz et al., 2018b; Holz et al., 2018a) were attributed to mucilage. For instance, increased soil water retention in the rhizosphere of maize and lupin was attributed to the high water retention of mucilage (Carminati et al., 2010; Ahmed et al., 2014). Upon rewetting of dry rhizosphere, reduced soil moisture (Moradi et al., 2012; Carminati,

* Corresponding author.
E-mail address: pascal.benard@usys.ethz.ch (P. Benard).

https://doi.org/10.1016/j.geoderma.2023.116576
Received 30 November 2022; Received in revised form 26 April 2023; Accepted 18 June 2023
Available online 4 July 2023

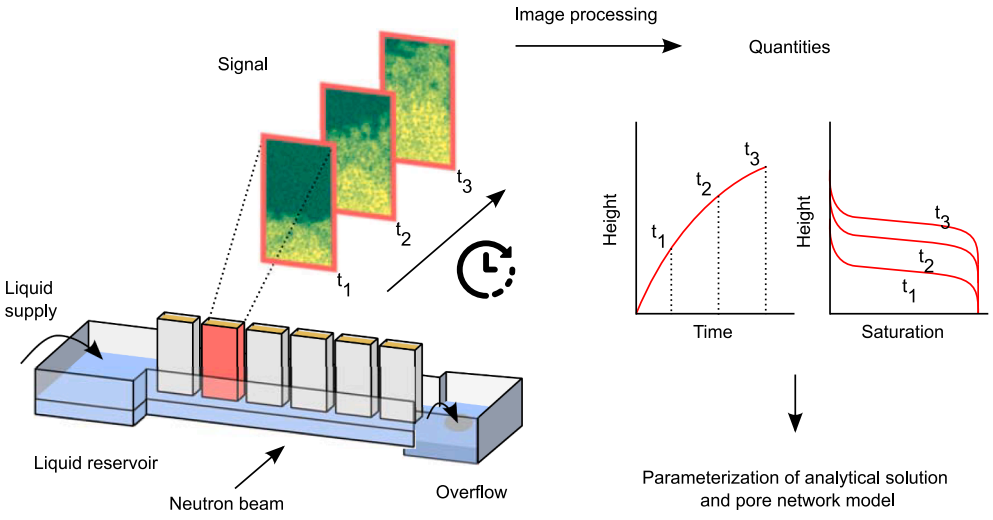

Fig. 1. Illustration of experimental procedure of time-series neutron radiography imaging (consecutive time steps indicated by t_1-t_3) and analysis of capillary rise of ethanol and water. The neutron beam is attenuated by the sample material and the imbibing liquid while the penetrating signal is captured by a detector. Through image processing the signal is translated into a 2D distribution of liquid thickness perpendicular to the sample. Derived dynamics of liquid distribution are used to parameterize the analytical solution of the Lucas-Washburn equation (Liu et al., 2016) and the pore network model.

2013; Ahmed et al., 2016) and root water uptake (Zarebanadkouki and Carminati, 2014; Zarebanadkouki et al., 2018) were observed over extended periods. These effects were correlated with a reduction of mucilage wettability upon drying (Kroener et al., 2015; Benard et al., 2016; Ahmed et al., 2016). The soil moisture-dependent occurrence of water repellency in the rhizosphere is not exclusive to this soil region but it is a common observation in various soil environments (Bachmann et al., 2007). Heterogeneous distribution of dry mucilage structures within the soil pore space has been emphasized to be a most relevant parameter controlling the threshold-like switch in macroscopic wettability and the percolative nature of the infiltration process (Benard et al., 2018a). The preferential distribution of mucilage in contact regions between soil particles (Benard et al., 2018b) is the product of its distinct physical properties and liquid movement in drying soils. With an increase in mucilage concentration, water potential in the liquid phase decreases (McCully and Boyer, 1997) and so does surface tension while viscosity increases (Read and Gregory, 1997; Read et al., 1999; Naveed et al., 2019; Benard et al., 2021). These properties induce an increase in liquid connectivity and eventually result in the creation of stable polymeric structures extending across the pore space when soil dries. This mechanism delays the fragmentation of the liquid phase (Albalasmeh and Ghezzehei, 2014; Carminati et al., 2017; Benard et al., 2019, 2021; Williams et al., 2021) and can reduce gas diffusion (Haupenthal et al., 2021). These and other soil hydraulic modifications are EPS-concentration dependent. For example soil hydraulic conductivity decreases while soil water retention increases with EPS concentration (Volk et al., 2016; Kroener et al., 2018; Zheng et al., 2018).

The ecological relevance of increased soil water retention, enhanced liquid connectivity and modifications of soil wettability in dry rhizosphere, however, are only partly understood. While a delayed fragmentation of the liquid phase (Carminati et al., 2017) and increased soil water retention were linked to enhanced nutrient (Zarebanadkouki et al., 2019) and enzyme diffusion (Holz et al., 2019), little is known on the impact of reduced soil wettability on rhizosphere water dynamics which is caused by gaps in the mechanistic description of the process. Current knowledge is that dry mucilage reduces the initial wettability of solid surfaces (Benard et al., 2016; Ahmed et al., 2016). Further, wettability commonly increases with time of contact between water and affected surfaces (Leelamanie and Karube, 2009; Whelan et al., 2015; Zickenrott et al., 2016) which can further affect water flow dynamics (Wang and Wallach, 2020). Generally, the mediation of soil hydraulic properties by bacterial EPS inducing delayed drying (Benard et al., 2023) and rewetting of soil (Or et al., 2007) helps to extend periods of biological activity (Skopp et al., 1990; Or et al., 2007; Benard et al., 2023).

So far, methodological approaches have not allowed differentiating between the impact of structural changes i.e., alteration of pore geometry vs. modifications of local initial wettability distribution induced by mucilage (Kroener et al., 2015; Benard et al., 2016, 2018a; Ahmed et al., 2016). Hence, the objective of this study was to quantify simultaneously the contribution of both alterations affecting water flow separately and in combination. Furthermore, the aim was to evaluate the impact of heterogeneities in wettability distribution on the rewetting process.

In this study, we utilized time-series neutron radiography to capture the capillary rise of both ethanol and water in sand treated with mucilage. By use of ethanol and water, geometric alterations of the pore space were distinguished from wettability induced modifications and the early rewetting process was captured. Results were used to parameterize a pore network model and subsequently assess the impact of wettability distribution. Outcomes were compared with results calculated using an analytical solution (Fries and Dreyer, 2008; Liu et al., 2016) of the Lucas-Washburn equation (Lucas, 1918; Washburn, 1921). The in-situ contact angles were determined in a parallel study (Schlüter et al., 2022).

2. Materials and methods

2.1. Experimental set-up

The impact of pore geometric alterations and wettability distribution on water imbibition was tested using mucilage amended sand. In this approach, sand was mixed with water and hydrated mucilage to create mucilage contents of 0.0, 0.1, 0.3, 0.6, 1.0, and 2.0 mg g^{-1} (mg dry mucilage per g of soil). As an analogue of plant root mucilage, chia mucilage (*Salvia hispanica*) extracted from seeds according to the description by Kroener et al. (2018) was used. The physical properties and the impact of chia mucilage on soil hydraulic properties are comparable to root-exuded mucilage regarding the magnitude of induced modifications (Segura-Campos et al., 2014; Naveed et al., 2019; Benard et al., 2021). All samples were prepared according to the following description. Acid washed, air-dried coarse sand (0.7–1.2 mm; SAND-SCHULZ GmbH, Berlin) was mixed with hydrated mucilage with an initial concentration of 6.97 mg g^{-1} to achieve a range of mucilage contents. To achieve a bulk density of the packing of 1.36±0.025 g cm^{-3} i.e., an approximate porosity of the final packing of 0.48, different amounts of hydrated mucilage and water were mixed with the respective weight of sand to achieve a minimum liquid saturation of ≥0.5 of the final packing. For a mucilage content of 2.0 mg g^{-1} the mixture was dried prior to packing to ensure 0.5 liquid saturation during packing. Porosity for treatments with 2.0 mg g^{-1} was slightly decreased with

0.44. For all other contents, deionized water was added to the mixture of hydrated mucilage and sand to achieve the minimum liquid saturation.

Treated sand was packed into aluminium containers of inner dimensions 0.6×1.6×3.0 cm which were sealed from one end with fiber tissue to enable capillary rise. Containers filled with mucilage-amended sand were dried by evaporation in a desiccator vessel filled with silica gel. Samples were dried until mass loss within one day was ca. ±1% of the approximate initial mass of water. Wet packing allows for an undisturbed distribution of mucilage in the pore space when soil dries (Benard et al., 2018b) inducing the characteristic alterations of soil pore geometry (Albalasmeh and Ghezzehei, 2014; Carminati et al., 2017; Benard et al., 2019). Note that a vertical redistribution of mucilage is highly unlikely in coarse sand as hydraulic conductivity diminishes at comparably high water content.

Capillary rise of ethanol and water was imaged using time-series neutron radiography. This method is highly sensitive to H-rich liquids, like water or ethanol in soil as they strongly attenuate neutrons (Moradi et al., 2009). For this reason, neutron radiography allows for non-invasively quantifying of liquid distribution at high temporal resolution (Carminati et al., 2007) by analysis of the difference between the signal of initially dry soil and wet soil. Time-series neutron radiography was conducted at the ICON (Imaging with COld Neutrons) beamline of the Paul Scherrer Institute, Villigen, Switzerland. A CCD camera with a field of view of 15×15 cm capturing the capillary rise of liquid at a pixel size of 58 μm was used. Acquired images were scatter corrected using a black body bias correction procedure (Boillat et al., 2018), normalized, spot cleaned and filtered (Kaestner and Schulz, 2015). Attenuation coefficients of water and ethanol were derived from liquid of specific thickness between the edge of aluminium containers and the aluminium channel (see Fig. 1) filled with the respective liquid to initiate liquid imbibition.

Capillary rise experiments were conducted by placing six aluminium containers in an aluminium channel connected to a liquid reservoir on one side and an overflow on the opposite side. In this way a constant liquid level during imbibition was ensured. Filling of the channel was initiated using a peristaltic pump filling the channel to a height of ca. 5 mm above the lower edge of containers. Capillary rise was imaged for three replicates of each mucilage content and liquid (ethanol and deionized water). The experimental procedure and derived quantities for analysis from time-series neutron radiography imaging are depicted in Fig. 1.

2.2. Analytical approach

The effective contact angle (CA) of sand was derived from the dynamics of the wetting front during capillary rise according to an analytical solution of the Lucas-Washburn equation (Fries and Dreyer, 2008; Liu et al., 2016). Including the impact of gravitational acceleration, the equation relates height of the wetting front and time by (1)

$$h = \frac{2\sigma\cos(\alpha)}{\rho g r \tau}\left(w\left(-exp\left(-1-\frac{t}{\frac{16\eta\sigma\cos(\alpha)}{\rho^2 g^2 r^3}}\right)\right)+1\right) \quad (1)$$

with height of the wetting front h [cm], surface tension of the liquid σ [mN m^{-1}], dynamic viscosity of the liquid η [g cm^{-1} s^{-1}], density of the liquid ρ [g cm^{-3}], effective CA α [degree], gravitational acceleration g [cm s^{-2}], effective pore radius r [cm], tortuosity factor τ [-], time t [s] and the Lambert W function w [–] (Corless et al., 1996). First, the effective geometric parameters r and τ were derived for each treatment by fitting the mean observed dynamics of ethanol imbibition of three replicates assuming $\alpha = 0°$ i.e., perfect wetting (Letey et al., 1962). Subsequently, the geometric parameters r and τ were used to match the relation of wetting front height and time of capillary rise of water using Eq. (1) by fitting α. Fitting of geometric parameters and effective CAs was done using Matlab 9.8.0.1396136 (R2020a; TheMathWorks, Inc., 2020). Note that for all treatments, dynamics of the ethanol front in the porous medium was evaluated for the initial ca. 30 s before the ethanol level in the aluminium channel below increased beyond the lower edge of containers. Similarly, at mucilage contents between 0.0 and 0.3 mg g^{-1}, the maximum height of water in the porous medium was reached before the water level in the channel increased. For mucilage contents ≥0.6 mg g^{-1}, the late phase of capillary rise above the submerged level of containers was included in the analysis. The height of the liquid front was derived for all treatments by manually thresholding the advancing liquid front from the difference between signals of wet images and the initial dry image.

Dynamics of water imbibition were analysed to evaluate the impact of mucilage on pore geometry and wettability. While the early phase of water imbibition is determined by the initial wettability and spatial distribution of mucilage structures, it is also affected by an increase in wettability upon contact of mucilage with water (Zickenrott et al., 2016) and at a time scale of minutes to days by the transport of water through rehydrating polymeric structures or swelling of dry mucilage (Chenu, 1993; Goerke et al., 2000; Singh et al., 2009). Water uptake of initially dry mucilage explains the slow rewetting of initially dry rhizosphere (Carminati et al., 2010). Note that the dynamics of wettability are not quantified in this study and related challenges and quantitative methods are discussed in the second last paragraph of the "Results and Discussion" section.

To compare the impact of initial wettability and pore geometry to other factors like increase in wettability and swelling of mucilage, the water saturation profile after 0.5 min, 1 min and 5 min (10 min for contents >0.6 mg g^{-1}) is compared for all treatments above the final water level in the aluminium channel.

The impact of spatially heterogeneous wettability distribution in combination with alterations of the pore geometry was analyzed using a site-bond invasion percolation model to simulate capillary rise of ethanol and water. Similar to the approach employing the analytical solution of the Lucas-Washburn equation, effective geometric parameters pore and throat size distribution were fitted by matching the dynamics of capillary rise of ethanol captured by time-series neutron radiography (i.e., saturation profile dynamics). Subsequently, the geometric parameters derived from ethanol imbibition dynamics of each treatment were used to evaluate different wettability distribution scenarios by matching the observed dynamics of water imbibition.

2.3. Numerical simulations

2.3.1. Pore network model

Capillary rise is simulated with an invasion site-bond percolation pore network model developed for this study. In the network, each site represents a pore that is placed on a cubic lattice connected via bonds that represent pore-throats with neighboring pores. The coordination number was 8, meaning each pore is connected to 8 of its adjacent neighbors unless it is situated at the edge of the numeric domain. In this case, individual coordination can be reduced. This coordination was chosen based on the relation of coordination and porosity presented by Dong and Blunt (2009). This modification is essential to capture saturation dynamics since the underestimation of pore coordination is likely to result in excessive air entrapment (Dong and Blunt, 2009).

The coordination of individual pores is randomly chosen from the 26 possible options as illustrated in Fig. A1. Throat sizes are distributed randomly in space and according to the derived global effective size distribution as explained in the parameterization section. Pore and throat size are correlated from smallest to largest beginning with the smallest mean diameter of all throats associated with the pore with the smallest diameter and so forth.

The pressure difference Δp [cm] inducing liquid flow from one pore to another is derived from the difference in capillary pressure according to the Young-Laplace equation (Young, 1804; Laplace, 1805) and gravitational acceleration (2)

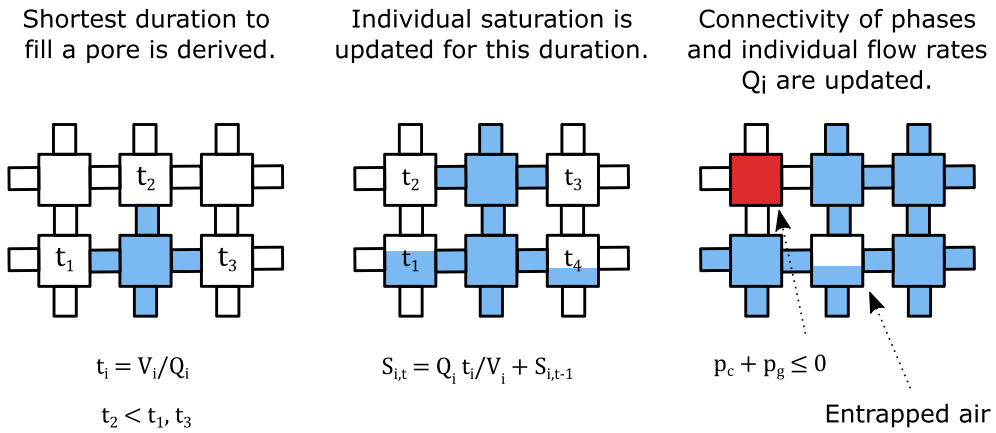

Fig. 2. Iteration process of liquid imbibition. The shortest time to saturate a pore is calculated according to Eq. (4) and individual pore saturation S_i accordingly. After each iteration, the connectivity of phases and flow rate Q_i is updated.

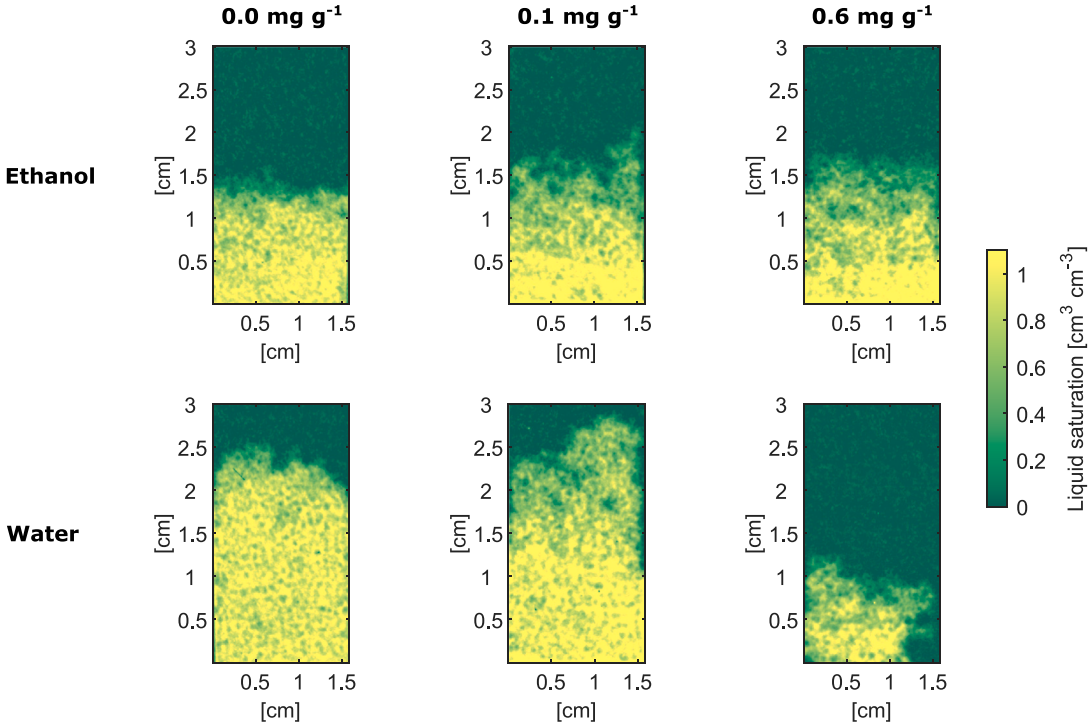

Fig. 3. Exemplary results of saturation distribution after 20 s of capillary rise of ethanol (top row) and water (bottom row) for mucilage content 0.0, 0.1, and 0.6 mg g^{-1} (from left to right).

$$\Delta p = -\frac{2\sigma}{r_{pore}}\cos(\alpha) + \rho g z \tag{2}$$

with liquid surface tension σ [mN m^{-1}], pore radius r_{pore} [cm], CA α [degree], liquid density ρ [g cm^{-3}], gravitational acceleration g [cm s^{-2}] and respective vertical elevation above the reference height of the free liquid z [cm]. Assuming flow Q [cm^3 s^{-1}] from a saturated pore into an unsaturated pore through a cylindrical pipe, the flow resistance is derived from the Hagen-Poiseuille equation (Hagen, 1839; Poiseuille, 1846) (3)

$$Q = \frac{\pi r_{throat}^4 \Delta p}{\eta 8 L} \tag{3}$$

with throat radius r_{throat} [cm], viscosity η [g cm^{-1} s^{-2}] and tube length L [cm]. The length of L is the sum of radii of connected pores multiplied by a factor to account for pore positions on the cubic lattice (see Fig. A1). This factor is 1 for pores facing each other (e.g., number 11), 1.41 for pores diagonal to each other on the same plane (e.g., number 14), and 1.73 for pores closest at a corner of the cubic lattice (e.g., number 3).

Integrating (2) into (3) the flow of liquid into an unsaturated pore Q_i [cm^3 s^{-1}] is calculated at each time step with the total flow resistance as the sum of individual resistances along the flow path according to (4).

$$Q_i = \left(\frac{2\sigma}{r_{pore}}\cos(\alpha) - \rho g z\right)\left(\frac{\pi}{8\eta}\left(\sum \frac{L}{r_{throat}^4}\right)^{-1}\right) \tag{4}$$

The time to saturate a pore t_i [s] is calculated according to (5)

$$t_i = \frac{V_i}{Q_i} \tag{5}$$

with specific pore volume V_i [cm^3]. V_i is calculated for a spherical volume derived from the pore radius r_{pore}.

The process of liquid imbibition is simulated for variable time steps

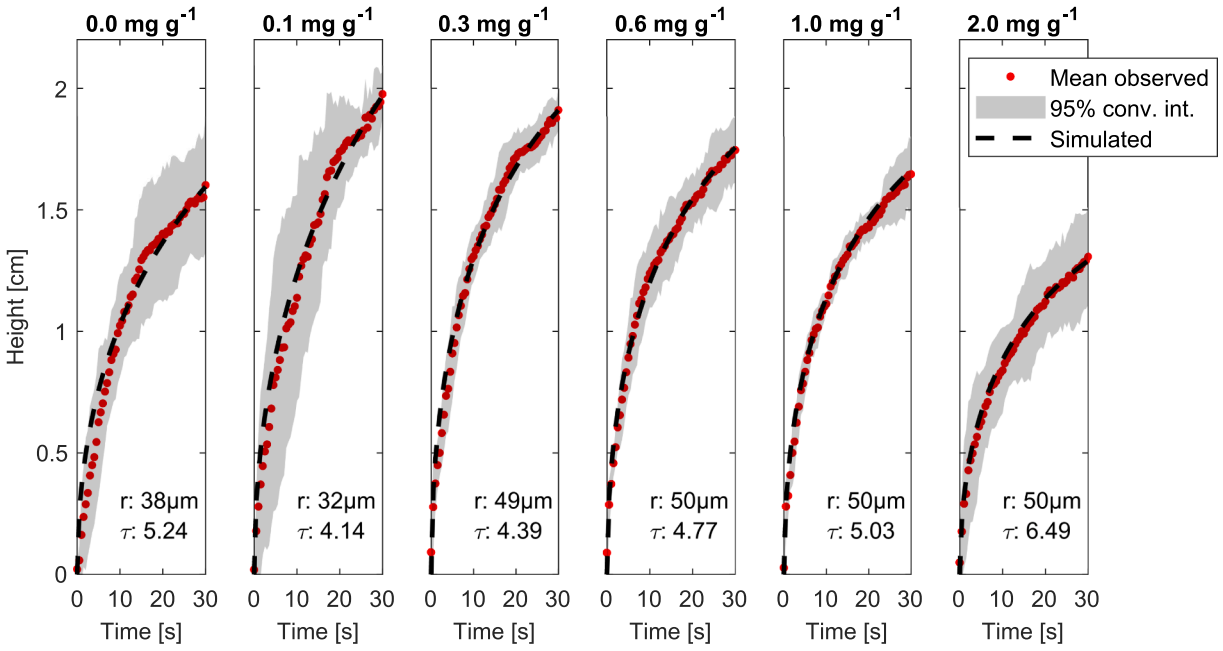

Fig. 4. Mean observed height of ethanol wetting front over time (red dots) for a range of mucilage content with 95% confidence interval of the mean (grey band) and results from the analytical solution of Eq. (1) (dashed black line) and respective geometric fitting parameters r (effective pore radius) and τ (tortuosity factor).

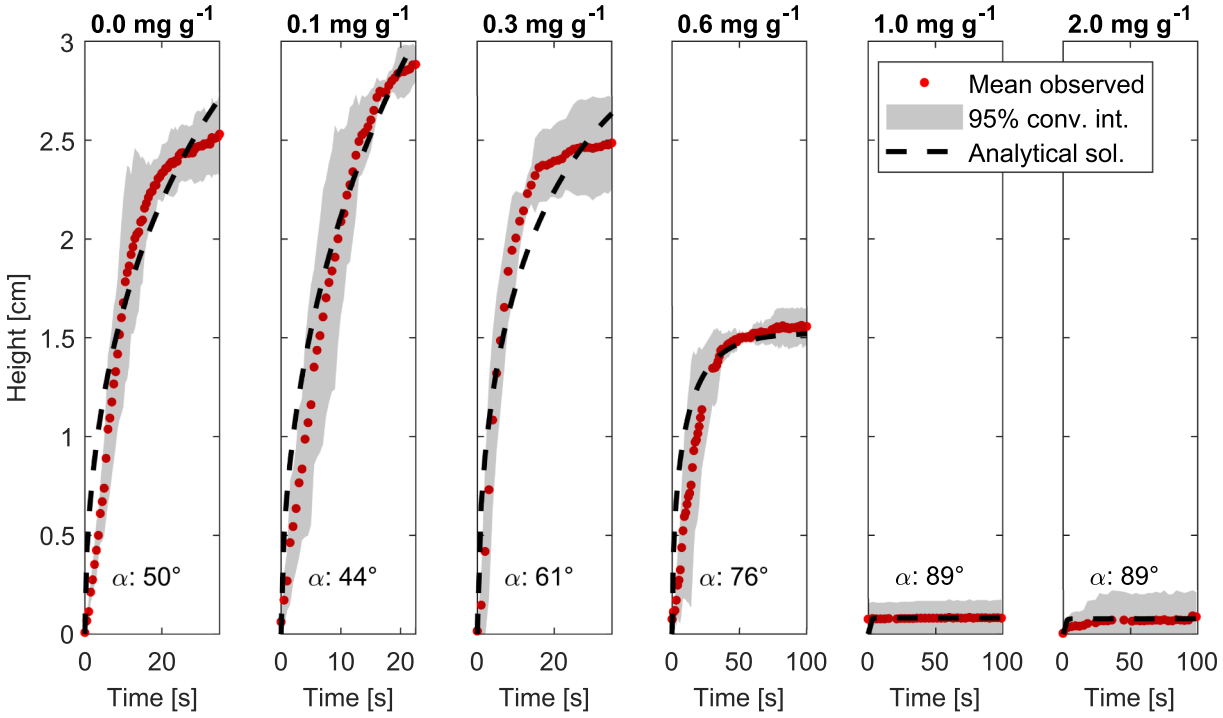

Fig. 5. Mean observed height of water wetting front over time (red dots) for a range of mucilage content with 95% confidence interval of the mean (grey band) and results from the analytical solution of eq.1 (dashed black line) for fitting parameter α (effective contact angle). Note that the x-axis limit is capped for 0.1 mg g^{-1} when the maximum height of capillary rise occurred and was adapted to display the near maximum height of capillary rise for all other treatments.

S. The shortest time to saturate a pore is derived based on the comparison of individual volumes V_i and current flow rates Q_i. For the shortest duration or time step, the saturation of all pores is updated according to Q_i and individual saturation from the previous time step $S_{i,t-1}$. After a pore is saturated, the connectivity of phases is reevaluated, and individual Q_i are updated (Fig. 2). A pore can only be filled if continually connected to air and water i.e., an air filled cluster of pores connecting to the surface of the numeric domain, and a cluster of liquid saturated pores connecting to the bottom of the numeric domain exists.

2.3.2. *Parameterization*

The initial effective pore and effective throat size distribution assigned to sites and bonds randomly in space, were derived by matching the saturation profile of ethanol for three replicates of the unamended control sand at 5 and 30 s with a two-parameter Weibull distribution function. Subsequently, the ethanol saturation profiles of

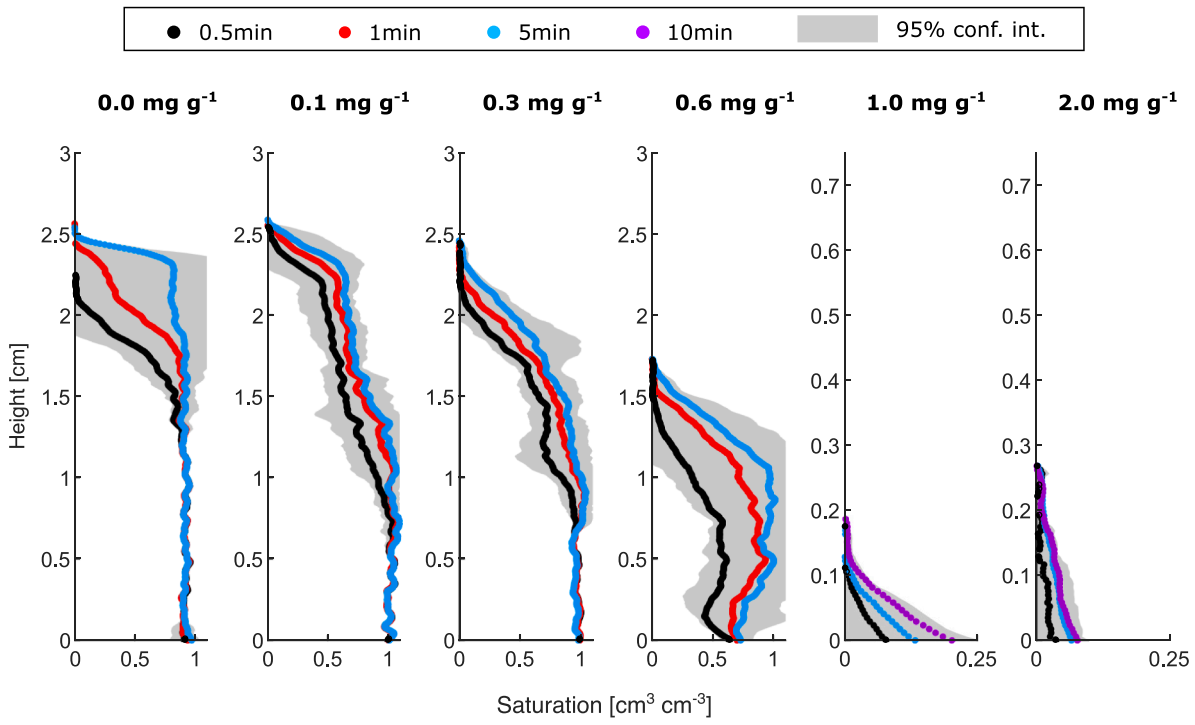

Fig. 6. Observed mean (n = 3) water saturation profiles above the height of water in the aluminum channel with 95% confidence interval of the mean after capillary rise in sand of different mucilage content at 0.5, 1 and 5 min (0.0–0.6 mg g^{-1}), and 0.5, 5 and 10 min (1.0 a. 2.0 mg g^{-1}). Note the different x- and y-axis limits for 1.0 a. 2.0 mg g^{-1}.

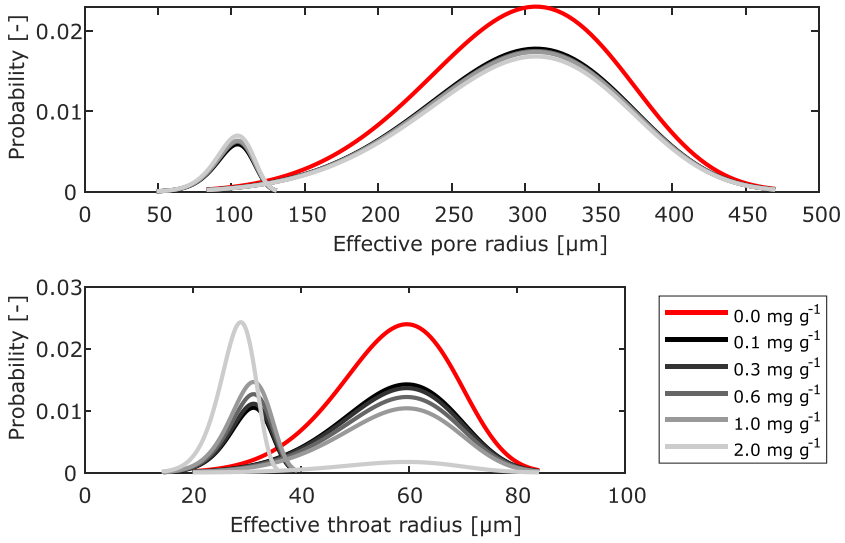

Fig. 7. Effective pore radius and effective throat radius distributions fitted for pore network model simulations with left shifted fractions for mucilage content >0.0 mg g^{-1} representing geometric pore space modifications.

mucilage amended treatments were matched by shifting a fraction of the original pore and throat sizes to a reduced size range i.e., a second Weibull distribution. The fraction of shifted pore and throat sizes were fitted to match the observed dynamics of capillary rise of ethanol while the range of the shifted size distribution function was fixed. This scheme was chosen to account for the non-uniform distribution of mucilage in bottlenecks of the soil pore space observed previously (Benard et al., 2018b; Benard et al., 2019). Perfect wettability i.e., a CA of 0° between particle surfaces and ethanol was assumed (Letey et al., 1962).

After derivation of the effective pore and effective throat size distribution by matching the observed ethanol imbibition, the effective CA distribution was estimated by matching observed and simulated water saturation profiles after 5 and 30 s of capillary rise. Four scenarios for spatial CA distribution were compared (S1-S4). Uniform wettability with the same CA assigned to all pores (S1); Normally distributed wettability between a minimum and a maximum CA with CAs randomly distributed in space (S2); Bimodal distribution of CA correlated with pore size (S3) from small to large and high to low CA; Bimodal distribution of CA with preferentially altered wettability in pores in contact to geometrically affected throats i.e., the fraction of pores affected by a shift in throat size distribution derived from matching ethanol capillary rise dynamics (S4). As a starting point to match observed water dynamics by fitting the wettability distribution in S3 and S4, the effective normal CA distribution of control treatments was used.

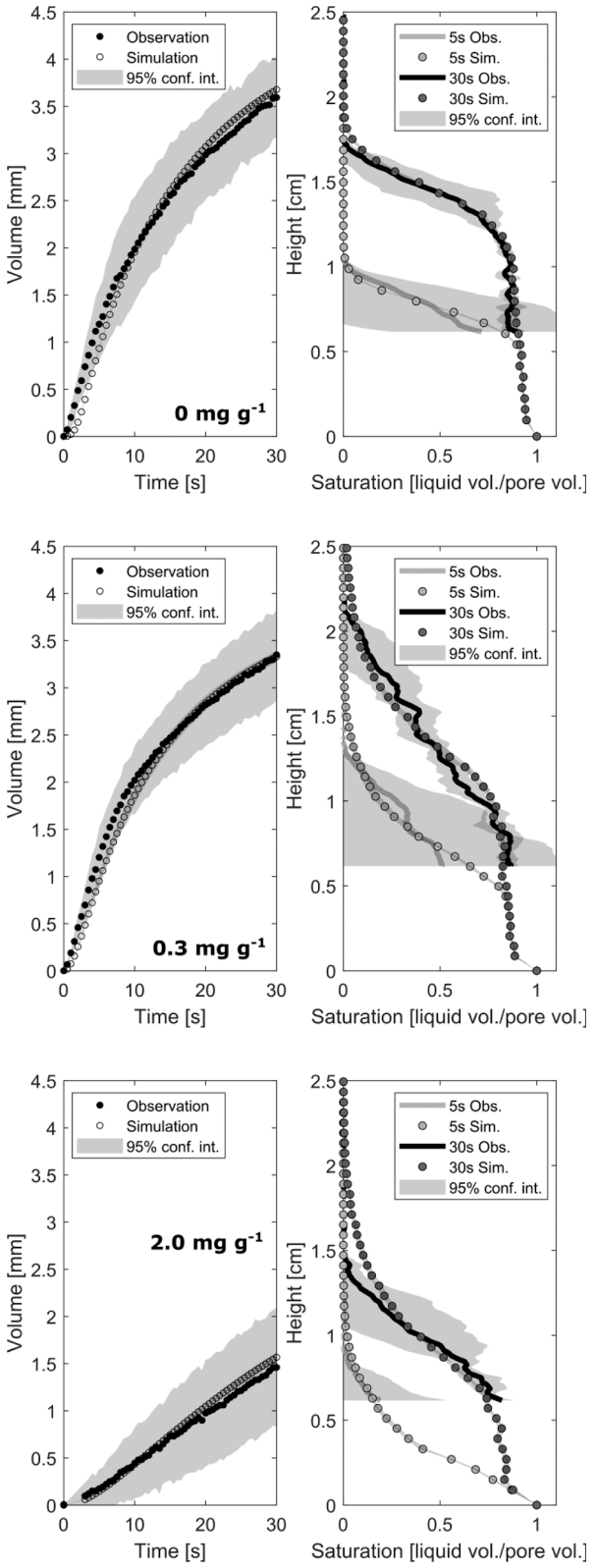

Fig. 8. Mean observed (n = 3) and simulated normalized volume of imbibed ethanol and ethanol saturation profiles at 5 and 30 s of capillary rise for different mucilage content with 95% confidence interval of the mean. Individual geometric parameters for each mucilage content were used (Fig. 7).

All simulations were made with a cross-sectional domain size of 20 by 20 pores. The sensitivity of the model to coordination number and cross-sectional area was tested for geometric parameters derived from ethanol imbibition at 0.0 mg g^{-1} (Fig. A2).

3. Results and discussion

A combination of methods was used to quantify the impact of mucilage on water flow in dry sand. Results from time-series neutron radiography of capillary rise of ethanol and water (Fig. 3) were used to derive the geometric parameters effective radius r and tortuosity factor τ which were subsequently used to fit the effective CA α using eq.1, an analytical solution of the Lucas-Washburn equation (Liu et al., 2016). To assess the principal impact of local alterations in wettability and modifications of pore geometry induced and their effect on rewetting, different wettability scenarios were compared using a pore network model.

Geometric parameters of the Lucas-Washburn equation, r and τ were derived by matching the dynamics of ethanol imbibition (height versus time). Observations are displayed along the result of the analytical solution in Fig. 4. At a mucilage content of 0.1 mg g^{-1} the advance of the liquid front was accelerated resulting in greater mean height which is reflected in the decrease of r and τ (Fig. 3 a. 4). At mucilage contents >0.3 mg g^{-1}, ethanol imbibition was increasingly decelerated with mucilage content manifested in an r of 50 μm and a continuous increase of τ to 6.5 at 2.0 mg g^{-1}.

Accelerated ethanol imbibition at low mucilage content (Fig. 3 a. 4) is likely related to an increase in pore connectivity due to mucilage structures created during drying, and bridging gaps between sand grains (Benard et al., 2018b). Such polymeric structures form when viscous mucilage delays the retreat of the liquid phase in drying soil and prevents the breakup of liquid connections (Carminati et al., 2017; Benard et al., 2021; Williams et al., 2021). This mechanism is not exclusive to plant and seed derived mucilage but was also observed for bacterial EPS (Zheng et al., 2018; Benard et al., 2019). The size of dry structures increases with mucilage content (Benard et al., 2018b) which eventually appear as 2D surfaces reaching across multiple pores (Benard et al., 2019). At comparably high mucilage content, these structures likely begin to limit the cross-section of accessible pore space for liquid transport. This mechanism explains the decelerated ethanol uptake by the porous medium at 2 mg g^{-1}, and could also explain the decrease in gas diffusion observed in mucilage amended soil (Haupenthal et al., 2021). Another explanation for accelerated ethanol imbibition at low mucilage content could be the reduction of average effective pore size resulting in increased capillary forces. A combination of decreased effective pore size and increased connectivity is supported by r and τ derived from fits of the analytical solution which decreased from 38 to 32 μm and 5.2 to 4.1, respectively.

The individual geometric parameters r and τ of each treatment i.e., mucilage content derived from ethanol imbibition dynamics were used to match observed water imbibition by fitting the effective CA α of eq.1 (Fig. 4). Like for ethanol, water imbibition was slightly accelerated at 0.1 mg g^{-1} (see also Fig. 3) and α was slightly reduced (Fig. 5). At 0.3 mg g^{-1}, mean height of water in the porous medium was decreased resulting in an increase in α from 44° to 61°. This trend persisted until α reached a maximum of >89° at ≥1.0 mg g^{-1}.

The decrease in α from 50° to 44° at 0.1 mg g^{-1} (Fig. 5) appears reasonable when compared to the minimum CA of mucilage treated glass surfaces and soil (Zickenrott et al., 2016; Ahmed et al., 2016; Benard et al., 2018b; a). It is interesting to note, that a reduction of CA during contact with water has recently been observed by Bachmann et al. (2021). It should be noted, that observed CA were still non-zero and also showed a rank order according to the initial CA of the dry material before contact with water. This confirms the equilibrium CAs in the capillary fringe obtained from X-ray CT imaging of sand treatments prepared as described in this study between 59° and 54° (Schlüter et al.,

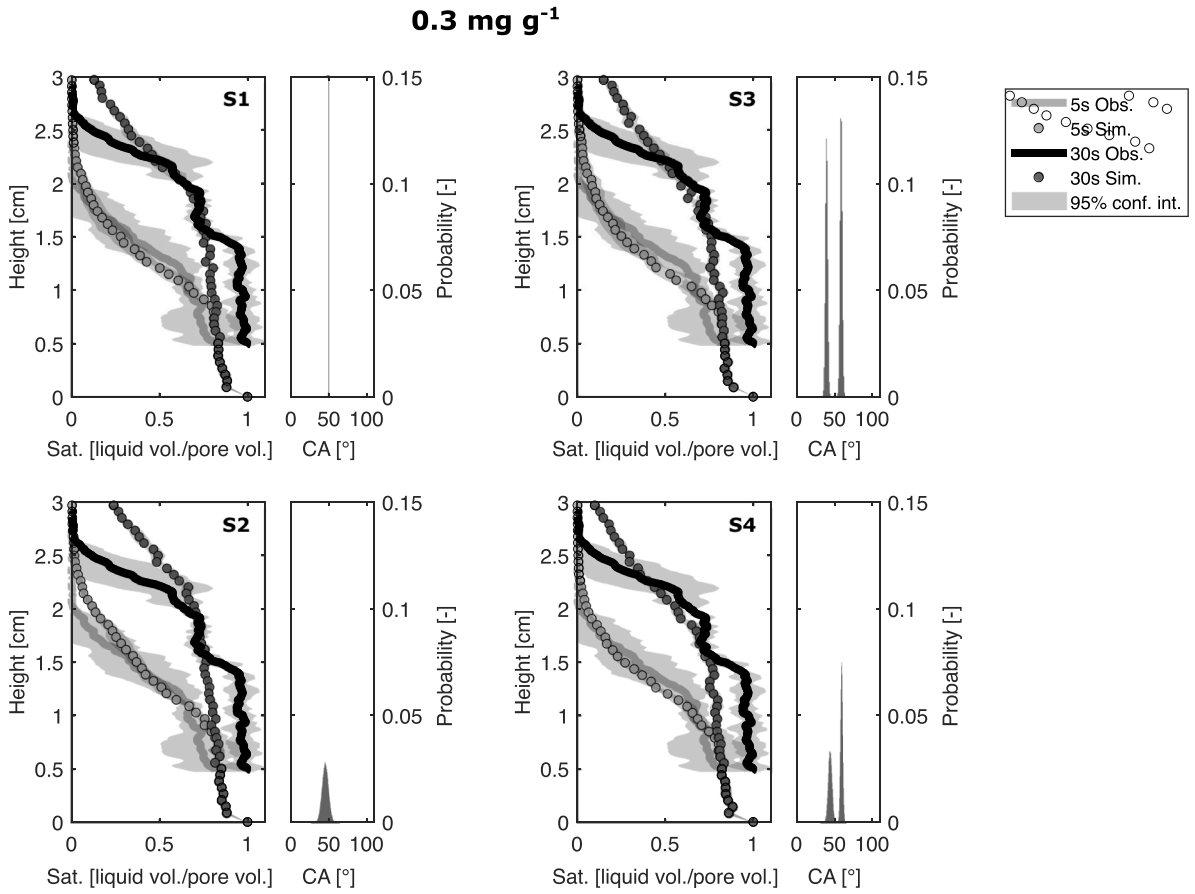

Fig. 9. Mean observed (n = 3) and simulated saturation profiles after 5 and 30 s of water imbibition with 95% confidence interval of the mean at mucilage content 0.3 mg g^{-1} along respective wettability distributions with scenarios S1 (uniform), S2 (normal random), S3 (bimodal assigned) a. S4 (bimodal unassigned i. e., random).

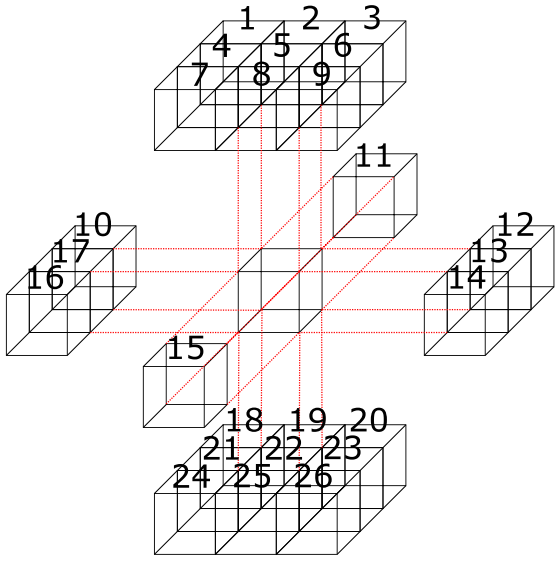

Fig. A1. Coordination scheme of pore positions on a cubic lattice represented by transparent cubes. Each number represent a potential connection between positioned pores with regard to the central position.

2022). At 0.3 mg g^{-1}, decreased wettability balanced alterations of the pore geometry resulting in similar water imbibition dynamics as observed in the control treatment. For mucilage contents >0.3 mg g^{-1} water imbibition was limited as shown exemplarily for 0.6 mg g^{-1} in Fig. 3. Derived τ increased while α decreased until capillary rise of water was prevented at mucilage content ≥1.0 mg g^{-1}. The increase in τ is consistent with previous studies reporting an increase in size of mucilage structures deposited in bottlenecks of the soil pore space (Benard et al., 2018a) which lead to an increase in average flow path length. The limitation of water imbibition to the first few millimetres at mucilage content ≥1.0 mg g^{-1} is the result of this process causing a decrease in accessible pore space and effective wettability. These observations are in line with results from X-ray CT imaging which showed reduced capillary rise due to water infiltration in a few pores at mucilage content of 1.0 mg g^{-1} (Schlüter et al., 2022). Note that water flow across the rhizosphere might occur in these conditions, as the size of the soil layer affected by mucilage is not expected to exceed a few millimeters away from the root surface. Differences between the analytical solution and observed capillary rise dynamics, especially for mucilage content ≤0.3 mg g^{-1} (Fig. 5) are likely the result of time dependent changes in CA (Leelamanie and Karube, 2009; Zickenrott et al., 2016). The impact of this phenomenon and potential methods of quantification are discussed with the results from pore-network simulations in the second last paragraph of this section.

The dynamics of water saturation showed reduced rewetting rates for mucilage amended treatments with time. Saturation profiles for each treatment are shown for the height above the water table in the aluminum channel in Fig. 6. An increased water content was observed for 0.1 mg g^{-1} in mucilage content below 1.3 cm in height. This effect might in part be the result of minor differences in porosity. Above this height, the water content decreased gradually and remained reduced after 5 min when compared to the control. For mucilage content >0.1 mg g^{-1} saturation was similarly decreased above 1 cm in height and for

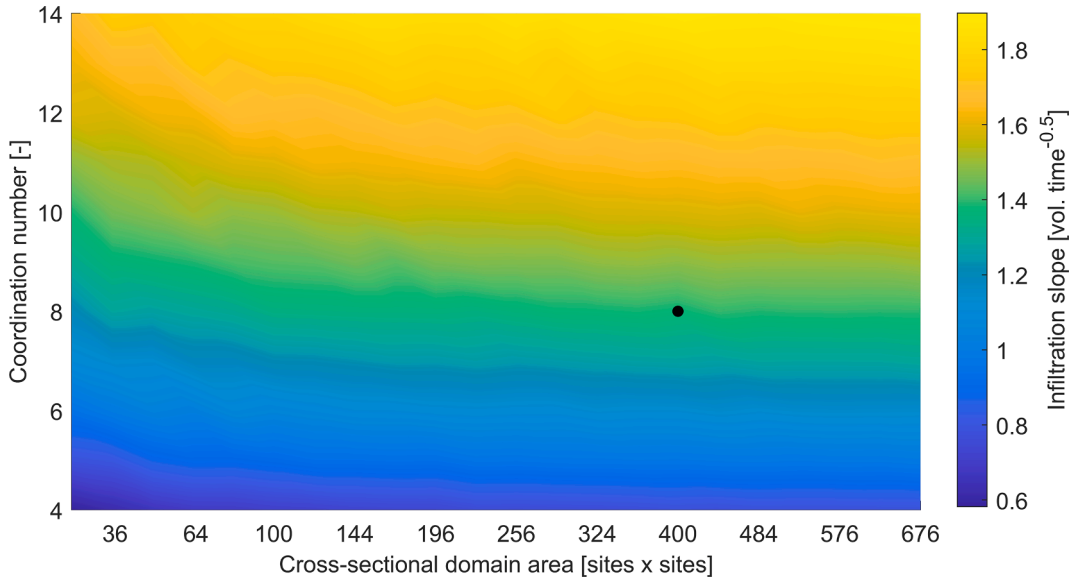

Fig. A2. Sensitivity of imbibition dynamics of pore-network model for parameter pair coordination number and cross-sectional area. Simulations were done with a coordination number of 8 and a cross-sectional area of 400 indicated by the black dot.

0.6 mg g^{-1} reduced saturation was observed starting from 0 cm (see Fig. 3 for an exemplary 2D illustration). For 1.0 mg g^{-1}, saturation was greatly decreased to a mean maximum height of 0.2 cm after 10 min. At 2.0 mg g^{-1} only a slight increase in water content occurred within the first 0.27 cm.

The analysis of water saturation profiles shows an increased length of the liquid front i.e., the interface between liquid and gas phase at a mucilage content of 0.1 mg g^{-1} (Fig. 6). Progressive rewetting along the liquid front was observed in presence of mucilage. Increased water saturation within the first cm at 0.1 mg g^{-1} indicates a balancing effect of induced modifications resulting in reduced air entrapment. Entrapment of air is likely to occur in sand as large unsaturated pores are easily bypassed during capillary rise. An increase in pore connectivity as discussed earlier might as well contribute to saturating large pores before being cut off from the gas phase. The increase in saturation within the first 5 min at a height $\geq$1.7 cm in the control treatment is likely related to an increase in local wettability of particle surfaces adjoining the wetting front. Reduction of CA during contact with water was also observed by Bachmann et al. (2021). In this context, the comparably big change in saturation across the rewetted profile at 0.6 mg g^{-1} indicates a large contact area between water and initially non-wettable pore space and/or non-zero CA even in the wetted state. For mucilage content $\geq$1.0 mg g^{-1}, water imbibition appeared to be dominated by slow rehydration (i.e., swelling) of dry mucilage. It is worth noting, that the equilibration time, before in situ contact angle measurements of same treatments were conducted had to be increased from 5 to 130 min between 0.0 and 2.0 mg g^{-1} in order to establish a capillary fringe with ca. 50% liquid saturation (Schlüter et al., 2022). Nevertheless, the measured CAs were very similar to those in control treatments despite the increasing equilibration time needed. This observation highlights the impact of properties other than wettability like rehydration of mucilage in bottlenecks of the pore space in controlling the rewetting process. Especially in light of the decrease in CA reported for mucilage treated surfaces (Zickenrott et al., 2016) and in the rhizosphere (Moradi et al., 2012) occurring on a time scale of seconds in contrast to a reduced water content of dry rhizosphere persisting for several hours (Zarebanadkouki and Carminati, 2014; Zarebanadkouki et al., 2018), emphasize the importance of pore space alteration including pore clogging induced by mucilage (Benard et al., 2018b) and other potential EPS (Volk et al., 2016; Zheng et al., 2018).

As the connectivity of accessible pore space decreases due to continuous mucilage depositions indicated by reduced ethanol imbibition observed in this study and results obtained from other studies (Benard et al., 2018b; Haupenthal et al., 2021), the opposite effect on connectivity is to be expected in drying soil. In other words, when mucilage is concentrated in drying soil, its water retention is enhanced (McCully and Boyer, 1997; Read et al., 1999) and liquid connectivity throughout the pore space is preserved (Carminati et al., 2017; Williams et al., 2021). Although liquid connectivity has not been investigated in this study, presented results provide further evidence supporting the hypothesis of improved liquid continuity in the rhizosphere (Carminati et al., 2017).

Employing a pore network model, the combined contribution of modifications of pore geometry and local wettability induced by mucilage was evaluated. Geometric parameters effective pore and throat radius at mucilage content >0.0 mg g^{-1} were derived by shifting a fraction of the original distribution to match ethanol infiltration dynamics (Fig. 7). While these shifts in effective pore size appeared minor with up to 0.25 at 2.0 mg g^{-1} the fraction of shifted effective throat sizes increased to 0.9 at 2.0 mg g^{-1}. The geometric parameters required to inform the model were derived by matching the saturation profiles of ethanol imbibition at 5 and 30 s.

Fitted ethanol imbibition dynamics for 0.0, 0.3 and 2.0 mg g^{-1} mucilage content from pore network model simulations are displayed along observations in Fig. 8. For all results, see Fig. A3. The length of the ethanol wetting front i.e., the slope of the saturation profile which can be interpreted as the length of the wetting front was increased for mucilage content between 0.1 and 1.0 mg g^{-1}. At 2.0 mg g^{-1} the length of the wetting front decreased, and the normalized imbibed volume was reduced from 3.6 mm to 1.5 mm in 30 s.

Pore-network model simulation of ethanol capillary rise were in good agreement with observations derived from neutron imaging. The model was able to match the dynamics of the process. The reduced imbibition observed for 2.0 mg g^{-1} could be reproduced, and can be explained by pore clogging at high mucilage content (Benard et al., 2019).

The impact of local wettability distribution was evaluated based on the four described scenarios (S1-S4). All distribution scenarios captured the capillary rise dynamics of water at a similar quality (Fig. A4 and A5). Even scenario S1, a uniformly distributed CA resulted in no substantial differences in imbibition dynamics when compared to other scenarios (e.g., for 0.3 mg g^{-1}, Fig. 9). The average contact angle (derived for S1)

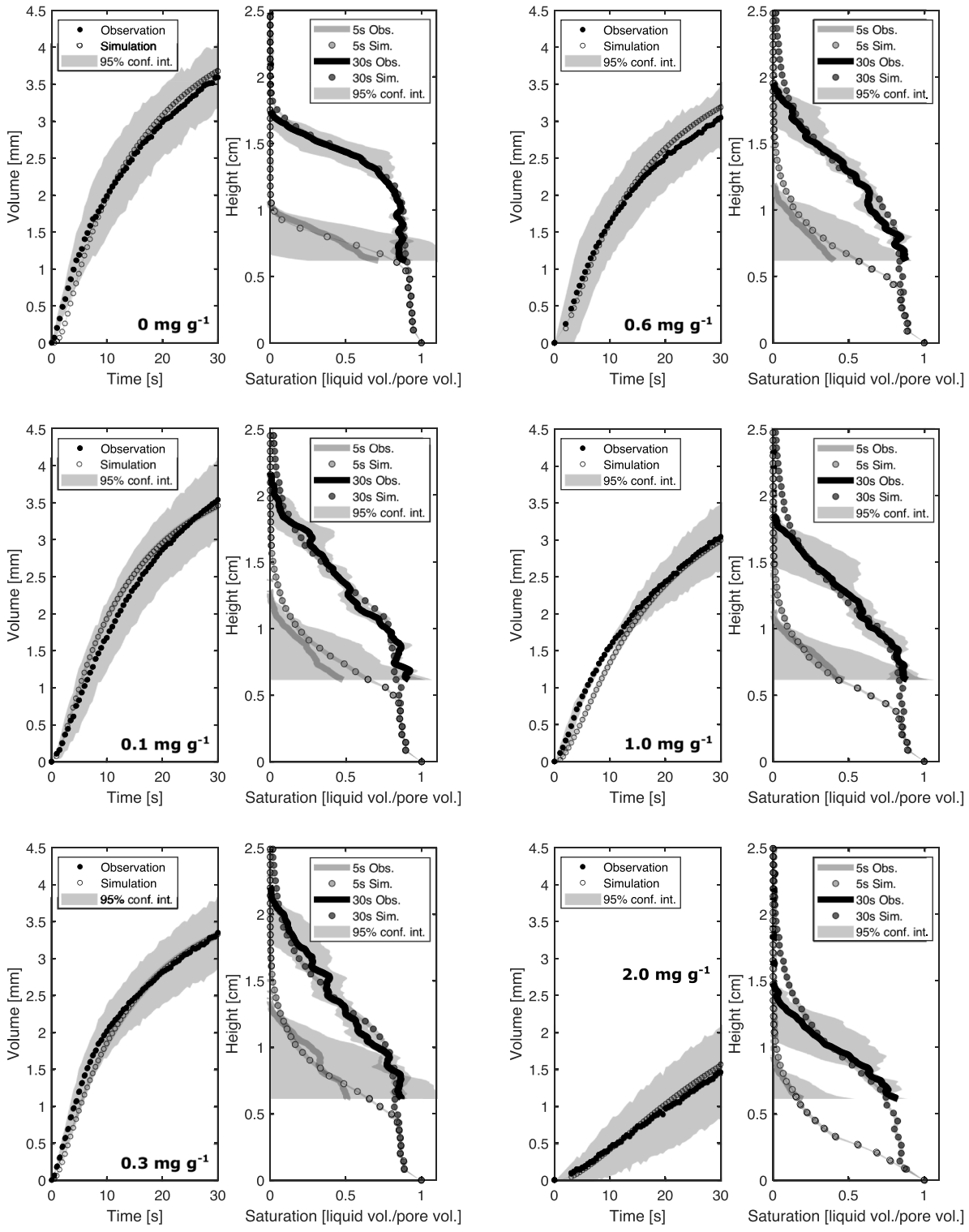

Fig. A3. Mean observed (n = 3) and simulated normalized ethanol imbibition and ethanol saturation profiles with 95% confidence interval of the mean at 5 and 30 s of capillary rise for different mucilage content.

decreased from 52.3° to 45° between 0.0 and 0.1 mg g^{-1} and increased thereafter to 50° and 66° at 0.3 and 0.6 mg g^{-1}, respectively. For the geometric parameters derived for 1.0 mg g^{-1} a minimum average contact angle of 84° prevented water imbibition beyond the observed elevation of ca. 0.1 cm (data not shown).

The distribution of local wettability had no substantial impact on water imbibition simulated with the pore network model (e.g., Fig. 9) which is likely due to the considerable impact of pore geometric alterations of the coarse sand. Additionally, temporal dynamics of wettability resulting in a decrease in CA of surfaces in contact with water which can substantially alter infiltration dynamics (Leelamanie and Karube, 2009; Whelan et al., 2015; Wang and Wallach, 2020) have not been considered. The employed methods do not allow to distinguish between the impact of static and dynamic contact angle or rehydration of mucilage depositions on the rewetting process. The in-situ time-resolved quantification of local wettability remains a great challenge in

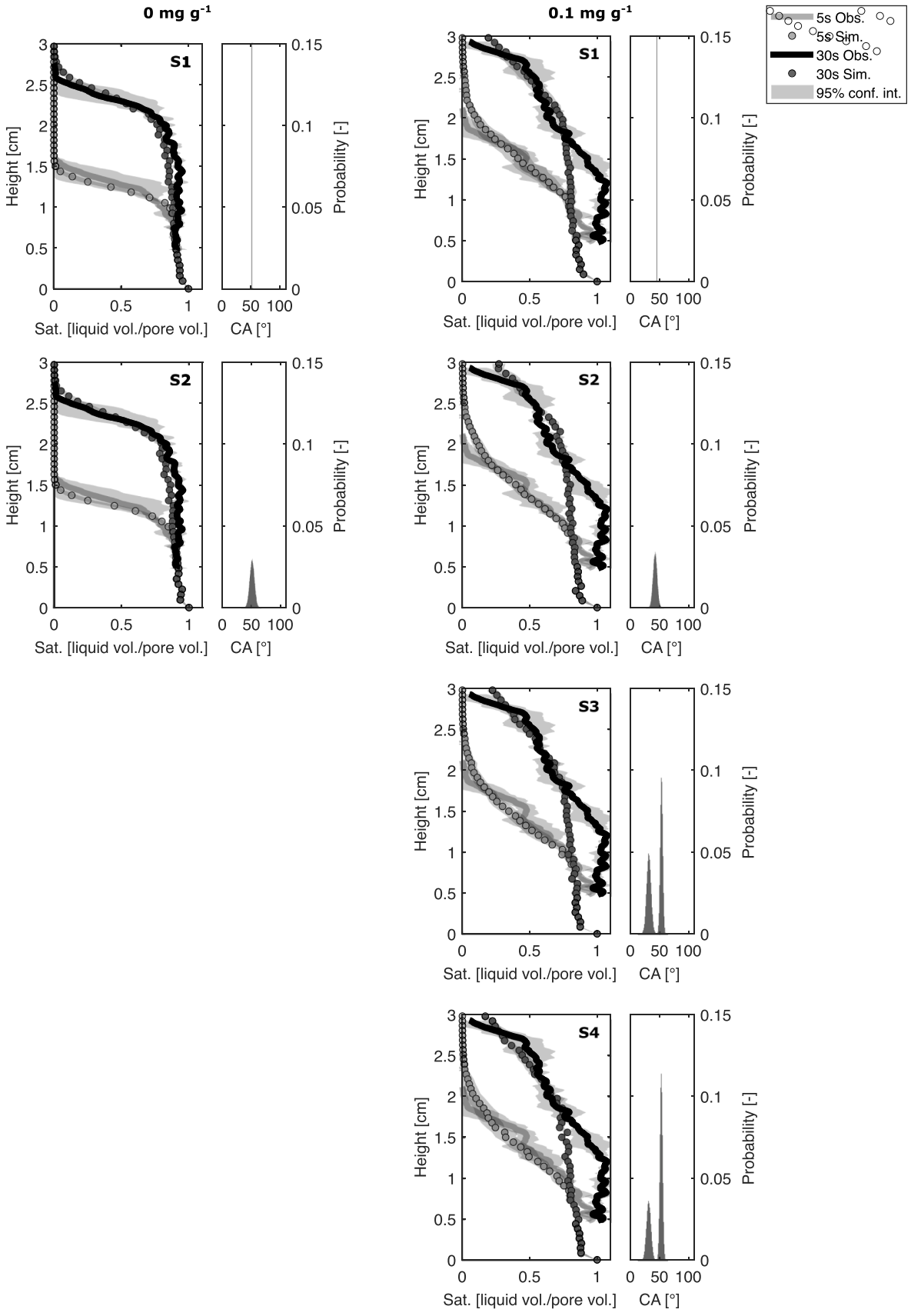

Fig. A4. Mean observed (n = 3) and simulated saturation profiles after 5 and 30 s of water imbibition with 95% confidence interval of the mean at mucilage content 0.0 and 0.1 mg g^{-1}. Simulated wettability distribution scenarios S1 (uniform), S2 (normal random), S3 (bimodal assigned) a. S4 (bimodal unassigned i.e., random).

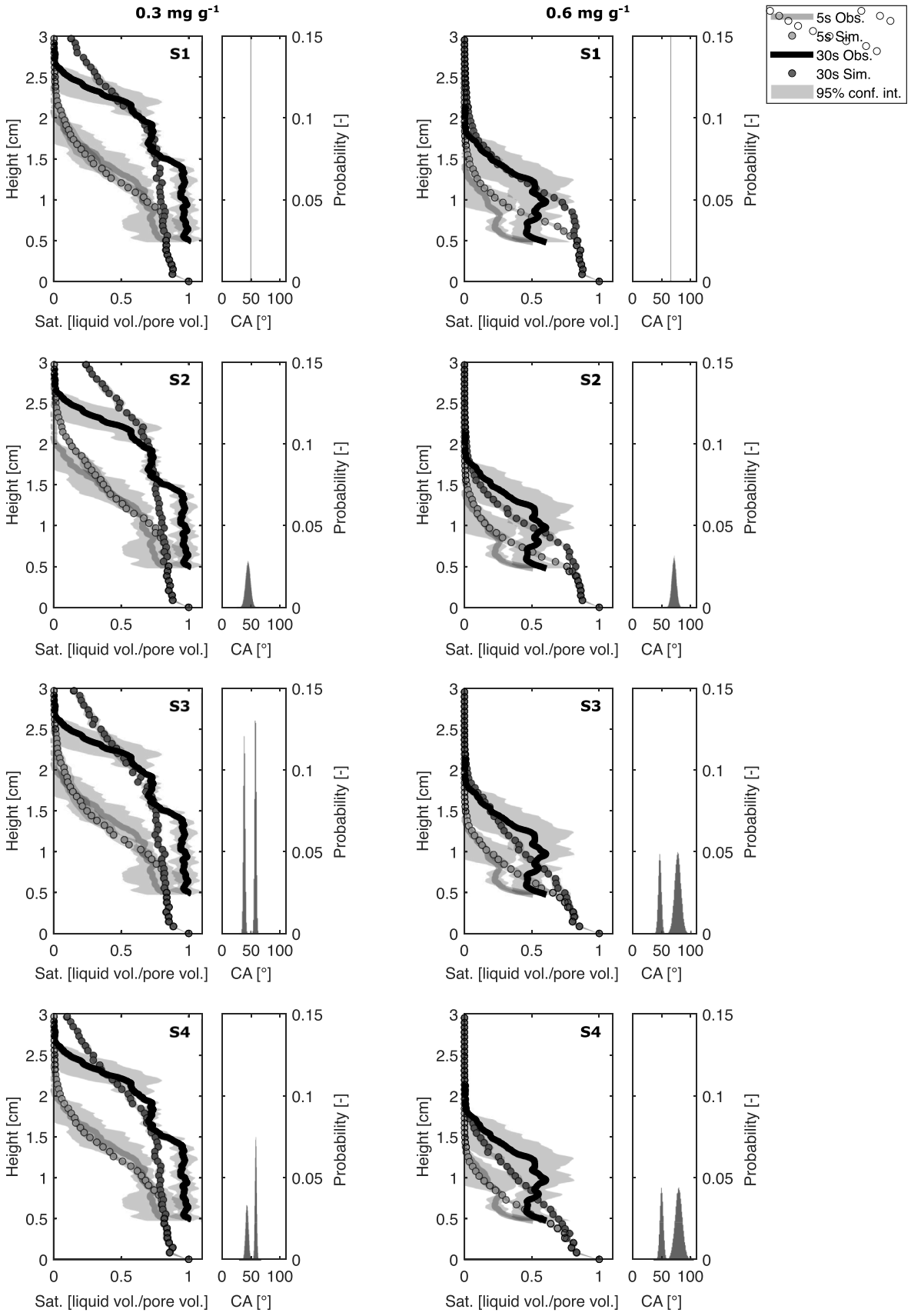

Fig. A5. Mean observed (n = 3) and simulated saturation profiles after 5 and 30 s of water imbibition with 95% confidence interval of the mean at mucilage content 0.3 and 0.6 mg g^{-1}. Simulated wettability distribution scenarios S1 (uniform), S2 (normal random), S3 (bimodal assigned) a. S4 (bimodal unassigned i.e., random).

this context. Especially since mucilage is non-uniformly distributed in soil (Benard et al., 2018b) and the wettability of dry mucilage may change over time (Zickenrott et al., 2016), therefore methods like X-ray CT are limited to near equilibrium conditions when changes in liquid configuration are much slower than image acquisition (Schlüter et al., 2022). The sessile drop method developed for soil (Bachmann et al., 2000) could be used to assess wettability dynamics of mucilage amended soils after breaking particles apart (Benard et al., 2018b). In undisturbed soils where the local distribution of mucilage structures and wettability are preserved, observations are limited to CA $\geq 90°$ while infiltration of the water droplet occurs rapidly below this value.

Although, the mean CA in all simulated scenarios was similar, a uniform wettability distribution seems unlikely considering the heterogeneous distribution of mucilage observed earlier (Benard et al., 2019). The employed pore network model could be improved by incorporating a time dependent CA relation and a function to describe the rehydration of mucilage accounting for slow water transport in clogged pores.

4. Conclusions

This study shows for the first time how macroscopic wettability is modified by alterations of pore structure and wettability in presence of mucilage. So far, decreased rhizosphere wettability was entirely explained by water repellent dry mucilage neglecting its potential impact on pore geometry (Benard et al., 2018a). Here, we have clarified the additional effects of the altered pore geometry. Enhanced pore connectivity at comparably low mucilage content facilitated water flow while accompanied by decelerated rewetting along an increased wetting front length (Fig. 5 a. 6). With an increase in mucilage content, flow resistance was increased reflected in an increased tortuosity from the analytical solution (Fig. 4) and decreased effective throat size from corresponding fits of the pore network model (Fig. 7). From an ecological perspective, observed reduced initial wettability for mucilage content >0.1 mg g^{-3}, progressive rewetting and an increase in wetting front length could be beneficial for numerous reasons. Reduced initial wettability helps to prevent anoxic conditions near the root surface which could not only harm the plant but could also reduce microbial activity (Skopp et al., 1990). On the other hand, as the soil region influenced by mucilage is unlikely to extend beyond a few millimeters (Holz et al., 2018b; Holz et al., 2018a), it is possible that water percolates through the rhizosphere despite a large fraction of water repellent pores, as for the capillary rise experiment in samples with high mucilage content (1.0 a. 2.0 mg g^{-1}; Fig. 5).

Microbial activity could further benefit from slow rewetting as is would allow the microbial community to adapt to changing moisture conditions and would avoid exposure to harmful gradients in osmotic potential due to the presence of rainwater (Or et al., 2007). Controlled rewetting along an extended wetting front could be a mechanism to optimize nutrient diffusion, microbial activity, and quantity of plant available resources by improving soil aeration while permitting preferential water flow to the root surface.

Overall, this study confirmed that micro-hydraulic properties and water flux in the rhizosphere can be captured by the chosen model approach that parametrized changes in pore geometry as well as changes in wettability on the pore scale. Further approaches are needed to incorporate time dependent parameters, like contact angle and rehydration of mucilage, to upscale these results to the root zone and to extend them to other soil textures and structures.

Declaration of Competing Interest

The authors declare that they have no known competing financial interests or personal relationships that could have appeared to influence the work reported in this paper.

Data availability

Data will be made available on request.

Acknowledgements

Financial support provided by the German Research Foundation DFG (316989341 and 403640522) for this project is greatly appreciated. Open access funding provided by ETH Zurich.

Appendix A

Fig. A1 – A5.

References

Ahmed, M.A., Kroener, E., Holz, M., Zarebanadkouki, M., Carminati, A., 2014. Mucilage exudation facilitates root water uptake in dry soils. Functional Plant Biol. 41 (11), 1129. https://doi.org/10.1071/FP13330.

Ahmed, M.A., Kroener, E., Benard, P., Zarebanadkouki, M., Kaestner, A., Carminati, A., 2016. Drying of mucilage causes water repellency in the rhizosphere of maize: measurements and modelling. Plant Soil 407 (1–2), 161–171. https://doi.org/10.1007/s11104-015-2749-1.

Albalasmeh, A.A., Ghezzehei, T.A., 2014. Interplay between soil drying and root exudation in rhizosheath development. Plant Soil 374 (1–2), 739–751. https://doi.org/10.1007/s11104-013-1910-y.

Bachmann, J., Ellies, A., Hartge, K.H., 2000. Development and application of a new sessile drop contact angle method to assess soil water repellency. Journal of Hydrology 231–232, 66–75. https://doi.org/10.1016/S0022-1694(00)00184-0.

Bachmann, J., Deurer, M., Arye, G., 2007. Modeling Water Movement in Heterogeneous Water-Repellent Soil: 1. Development of a Contact Angle-Dependent Water-Retention Model. Vadose Zone Journal 6 (3), 436–445. https://doi.org/10.2136/vzj2006.0060.

Bachmann, J., Söffker, S., Sepehrnia, N., Goebel, M., Woche, S.K., 2021. The effect of temperature and wetting–drying cycles on soil wettability: Dynamic molecular restructuring processes at the solid–water–air interface. Eur. J. Soil Sci. 72, 2180–2198. https://doi.org/10.1111/ejss.13102.

Benard, P., Kroener, E., Vontobel, P., Kaestner, A., Carminati, A., 2016. Water percolation through the root-soil interface. Advances in Water Resources 95, 190–198. https://doi.org/10.1016/j.advwatres.2015.09.014.

Benard, P., Zarebanadkouki, M., Carminati, A., 2018a. Impact of Pore-Scale Wettability on Rhizosphere Rewetting. Front. Environ. Sci. 6, 16. https://doi.org/10.3389/fenvs.2018.00016.

Benard, P., Zarebanadkouki, M., Hedwig, C., Holz, M., Ahmed, M.A., Carminati, A., 2018b. Pore-Scale Distribution of Mucilage Affecting Water Repellency in the Rhizosphere. Vadose Zone Journal 17 (1), 170013. https://doi.org/10.2136/vzj2017.01.0013.

Benard, P., Zarebanadkouki, M., Brax, M., Kaltenbach, R., Jerjen, I., Marone, F., Couradeau, E., Felde, V.J.M.N.L., Kaestner, A., Carminati, A., 2019. Microhydrological Niches in Soils: How Mucilage and EPS Alter the Biophysical Properties of the Rhizosphere and Other Biological Hotspots. Vadose Zone J. 18 (1), 1–10. https://doi.org/10.2136/vzj2018.12.0211.

Benard, P., Schepers, J.R., Crosta, M., Zarebanadkouki, M., Carminati, A., 2021. Physics of Viscous Bridges in Soil Biological Hotspots. Water Res 57 (11). https://doi.org/10.1029/2021WR030052.

Benard, P., Bickel, S., Kaestner, A., Lehmann, P., Carminati., A., 2023. Extracellular polymeric substances from soil-grown bacteria delay evaporative drying. Adv. Water Res. 172, 104364. https://doi.org/10.1016/j.advwatres.2022.104364.

Bengough, A.G., 2012. Water Dynamics of the Root Zone: Rhizosphere Biophysics and Its Control on Soil Hydrology. Vadose Zone Journal 11 (2), vzj2011.0111. https://doi.org/10.2136/vzj2011.0111.

Boillat, P., Carminati, C., Schmid, F., Grünzweig, C., Hovind, J., Kaestner, A., Mannes, D., Morgano, M., Siegwart, M., Trtik, P., Vontobel, P., Lehmann, E.H., 2018. Chasing quantitative biases in neutron imaging with scintillator-camera detectors: a practical method with black body grids. Opt. Express 26 (12), 15769. https://doi.org/10.1364/OE.26.015769.

Carminati, A., 2013. Rhizosphere wettability decreases with root age: a problem or a strategy to increase water uptake of young roots? Front. Plant Sci. 4 https://doi.org/10.3389/fpls.2013.00298.

Carminati, A., Moradi, A.B., Vetterlein, D., Vontobel, P., Lehmann, E., Weller, U., Vogel, H.-J., Oswald, S.E., 2010. Dynamics of soil water content in the rhizosphere. Plant Soil 332 (1–2),, 163–176. https://doi.org/10.1007/s11104-010-0283-8.

Carminati, A., Benard, P., Ahmed, M.A., Zarebanadkouki, M., 2017. Liquid bridges at the root-soil interface. Plant Soil 417 (1–2), 1–15. https://doi.org/10.1007/s11104-017-3227-8.

Carminati, A., Kaestner, A., Flühler, H., Lehmann, P., Or, D., Lehmann, E., Stampanoni, M., 2007. Hydraulic contacts controlling water flow across porous grains. Phys. Rev. E 76 (2), 026311. https://doi.org/10.1103/PhysRevE.76.026311.

Chenu, C., 1993. Clay- or sand-polysaccharide associations as models for the interface between micro-organisms and soil: water related properties and microstructure. Geoderma 56 (1–4), 143–156. https://doi.org/10.1016/0016-7061(93)90106-U.

Corless, R.M., Gonnet, G.H., Hare, D.E.G., Jeffrey, D.J., Knuth, D.E., 1996. On the LambertW function. Adv Comput Math 5 (1), 329–359. https://doi.org/10.1007/BF02124750.
Dong, H., Blunt, M.J., 2009. Pore-network extraction from micro-computerized-tomography images. Phys. Rev. E 80 (3), 036307. https://doi.org/10.1103/PhysRevE.80.036307.
Fries, N., Dreyer, M., 2008. An analytic solution of capillary rise restrained by gravity. Journal of Colloid and Interface Science 320 (1), 259–263. https://doi.org/10.1016/j.jcis.2008.01.009.
Goerke, U., Chamberlain, A.H.L., Crilly, E.A., McDonald, P.J., 2000. Model for water transport into powdered xanthan combining gel swelling and vapor diffusion. Phys. Rev. E 62 (4), 5353–5359. https://doi.org/10.1103/PhysRevE.62.5353.
Gregory, P.J., 2006. Roots, rhizosphere and soil: the route to a better understanding of soil science?: Roots, rhizosphere and soil. European Journal of Soil Science 57 (1), 2–12. https://doi.org/10.1111/j.1365-2389.2005.00778.x.
Hagen, G., 1839. Ueber die Bewegung des Wassers in engen cylindrischen Röhren. Ann. Phys. Chem. 122 (3), 423–442. https://doi.org/10.1002/andp.18391220304.
Hallett, P.D., Marin, M., Bending, G.D., George, T.S., Collins, C.D., Otten, W., 2022. Building soil sustainability from root–soil interface traits. Trends in Plant Science 27 (7), 688–698. https://doi.org/10.1016/j.tplants.2022.01.010.
Haupenthal, A., Brax, M., Bentz, J., Jungkunst, H.F., Schützenmeister, K., Kroener, E., 2021. Plants control soil gas exchanges possibly *via* mucilage. J. Plant Nutr. Soil Sci. 184 (3), 320–328. https://doi.org/10.1002/jpln.202000496.
Holz, M., Leue, M., Ahmed, M.A., Benard, P., Gerke, H.H., Carminati, A., 2018a. Spatial Distribution of Mucilage in the Rhizosphere Measured With Infrared Spectroscopy. Font. Environ. Sci. 6, 87. https://doi.org/10.3389/fenvs.2018.00087.
Holz, M., Zarebanadkouki, M., Kaestner, A., Kuzyakov, Y., Carminati, A., 2018b. Rhizodeposition under drought is controlled by root growth rate and rhizosphere water content. Plant Soil 423 (1–2), 429–442. https://doi.org/10.1007/s11104-017-3522-4.
Holz, M., Zarebanadkouki, M., Carminati, A., Hovind, J., Kaestner, A., Spohn, M., 2019. Increased water retention in the rhizosphere allows for high phosphatase activity in drying soil. Plant Soil 443 (1–2), 259–271. https://doi.org/10.1007/s11104-019-04234-3.
Kaestner, A.P., Schulz, M., 2015. Processing Neutron Imaging Data – Quo Vadis? Physics Procedia 69, 336–342. https://doi.org/10.1016/j.phpro.2015.07.047.
Kroener, E., Ahmed, M.A., Carminati, A., 2015. Roots at the percolation threshold. Phys. Rev. E 91 (4), 042706. https://doi.org/10.1103/PhysRevE.91.042706.
Kroener, E., Holz, M., Zarebanadkouki, M., Ahmed, M., Carminati., A., 2018. Effects of Mucilage on Rhizosphere Hydraulic Functions Depend on Soil Particle Size. Vadose Zone Journal 17 (1), 170056. https://doi.org/10.2136/vzj2017.03.0056.
Kuzyakov, Y., Blagodatskaya, E., 2015. Microbial hotspots and hot moments in soil: Concept & review. Soil Biology and Biochemistry 83, 184–199. https://doi.org/10.1016/j.soilbio.2015.01.025.
Laplace, P.S., 1805. Supplément au dixième livre du Traité de Mécanique Céleste.
Leelamanie, D.A.L., Karube, J., 2009. Time dependence of contact angle and its relation to repellency persistence in hydrophobized sand. Soil Science and Plant Nutrition 55 (4), 457–461. https://doi.org/10.1111/j.1747-0765.2009.00387.x.
Letey, J., Osborn, J., Pelishek, R.E., 1962. MEASUREMENT OF LIQUID-SOLID CONTACT ANGLES IN SOIL AND SAND. Soil Science 93 (3), 149–153. https://doi.org/10.1097/00010694-196203000-00001.
Liu, Z., Yu, X., Wan, L., 2016. Capillary rise method for the measurement of the contact angle of soils. Acta Geotech. 11 (1), 21–35. https://doi.org/10.1007/s11440-014-0352-x.
Lucas, R., 1918. Ueber das Zeitgesetz des kapillaren Aufstiegs von Flüssigkeiten. Kolloid-Zeitschrift 23 (1), 15–22. https://doi.org/10.1007/BF01461107.
McCully, M.E., Boyer, J.S., 1997. The expansion of maize root-cap mucilage during hydration. 3. Changes in water potential and water content. Physiol Plant 99 (1), 169–177. https://doi.org/10.1111/j.1399-3054.1997.tb03445.x.
Moradi, A.B., Conesa, H.M., Robinson, B., Lehmann, E., Kuehne, G., Kaestner, A., Oswald, S., Schulin, R., 2009. Neutron radiography as a tool for revealing root development in soil: capabilities and limitations. Plant Soil 318 (1–2), 243–255. https://doi.org/10.1007/s11104-008-9834-7.
Moradi, A.B., Carminati, A., Lamparter, A., Woche, S.K., Bachmann, J., Vetterlein, D., Vogel, H.-J., Oswald, S.E., 2012. Is the Rhizosphere Temporarily Water Repellent? Vadose Zone Journal 11 (3), vzj2011.0120. https://doi.org/10.2136/vzj2011.0120.
Naveed, M., Ahmed, M.A., Benard, P., Brown, L.K., George, T.S., Bengough, A.G., Roose, T., Koebernick, N., Hallett, P.D., 2019. Surface tension, rheology and hydrophobicity of rhizodeposits and seed mucilage influence soil water retention and hysteresis. Plant Soil 437 (1–2), 65–81. https://doi.org/10.1007/s11104-019-03939-9.
Oades, J.M., 1978. MUCILAGES AT THE ROOT SURFACE. Journal of Soil Science 29 (1), 1–16. https://doi.org/10.1111/j.1365-2389.1978.tb02025.x.
Or, D., Phutane, S., Dechesne, A., 2007. Extracellular Polymeric Substances Affecting Pore-Scale Hydrologic Conditions for Bacterial Activity in Unsaturated Soils. Vadose zone j. 6 (2), 298–305. https://doi.org/10.2136/vzj2006.0080.
Poiseuille, J., 1846. Recherches expérimentales sur le mouvement des liquides dans les tubes de très petits diamètres. Mémoires présentés par Divers Savants à l'Académie Royale des sciences de l'Institut de France 9, 433–544.
Read, D.B., Gregory, P.J., 1997. Surface tension and viscosity of axenic maize and lupin root mucilages. New Phytol 137 (4), 623–628. https://doi.org/10.1046/j.1469-8137.1997.00859.x.
Read, D.B., Gregory, P.J., Bell, A.E., 1999. Physical properties of axenic maize root mucilage. Plant and Soil 211 (1), 87–91. https://doi.org/10.1023/A:1004403812307.
Roberts, E.A., 1916. The Epidermal Cells of Roots. Botanical Gazette 62 (6), 488–506. https://doi.org/10.1086/331960.
Schlüter, S., Blaser, S.R.G.A., Benard, P., Carminati, A., 2022. In situ measurement of 3D contact angle in sand based on X-ray computed tomography. Vadose Zone Journal 21 (3). https://doi.org/10.1002/vzj2.20197.
Segura-Campos, M.R., Ciau-Solís, N., Rosado-Rubio, G., Chel-Guerrero, L., Betancur-Ancona, D., 2014. Chemical and Functional Properties of Chia Seed (*Salvia hispanica* L.) Gum. International Journal of Food Science 2014, 1–5. https://doi.org/10.1155/2014/241053.
Singh, K., Kumar, A., Langyan, N., Ahuja, M., 2009. Evaluation of Mimosa pudica Seed Mucilage as Sustained-Release Excipient. AAPS PharmSciTech 10 (4), 1121–1127. https://doi.org/10.1208/s12249-009-9307-1.
Skopp, J., Jawson, M.D., Doran, J.W., 1990. Steady-State Aerobic Microbial Activity as a Function of Soil Water Content. Soil Science Society of America Journal 54 (6), 1619–1625. https://doi.org/10.2136/sssaj1990.03615995005400060018x.
Volk, E., Iden, S.C., Furman, A., Durner, W., Rosenzweig, R., 2016. Biofilm effect on soil hydraulic properties: Experimental investigation using soil-grown real biofilm: HYDRAULIC PROPERTIES OF BIOFILM AMENDED SOIL. Water Resour. Res. 52 (8), 5813–5828. https://doi.org/10.1002/2016WR018866.
Wang, Z., Wallach, R., 2020. Effects of Time-Dependent Contact Angle on Wettability of Subcritically Water-Repellent Soils. Water Resour. Res. 56 (10) https://doi.org/10.1029/2020WR027314.
Washburn, E.W., 1921. The Dynamics of Capillary Flow. Phys. Rev. 17 (3), 273–283. https://doi.org/10.1103/PhysRev.17.273.
Whelan, A., Kechavarzi, C., Coulon, F., Doerr, S.H., 2015. Experimental characterization of the impact of temperature and humidity on the breakdown of soil water repellency in sandy soils and composts: IMPACT OF TEMPERATURE AND HUMIDITY ON SOIL WATER REPELLENCY BREAKDOWN. Hydrol. Process. 29 (8), 2065–2073. https://doi.org/10.1002/hyp.10305.
Williams, K.A., Ruiz, S.A., Petroselli, C., Walker, N., McKay Fletcher, D.M., Pileio, G., Roose, T., 2021. Physical characterisation of chia mucilage polymeric gel and its implications on rhizosphere science - Integrating imaging, MRI, and modelling to gain insights into plant and microbial amended soils. Soil Biology and Biochemistry 162. https://doi.org/10.1016/j.soilbio.2021.108404.
Young, T., 1804. An Essay on the Cohesion of Fluids. Philos. Trans. R. Soc. 95.
Zarebanadkouki, M., Ahmed, M., Hedwig, C., Benard, P., Kostka, S.J., Kastner, A., Carminati, A., 2018. Rhizosphere hydrophobicity limits root water uptake after drying and subsequent rewetting. Plant Soil 428 (1–2), 265–277. https://doi.org/10.1007/s11104-018-3677-7.
Zarebanadkouki, M., Carminati, A., 2014. Reduced root water uptake after drying and rewetting. Z. Pflanzenernähr. Bodenk. 177 (2), 227–236. https://doi.org/10.1002/jpln.201300249.
Zarebanadkouki, M., Fink, T., Benard, P., Banfield, C.C., 2019. Mucilage Facilitates Nutrient Diffusion in the Drying Rhizosphere. Vadose zone j. 18 (1), 1–13. https://doi.org/10.2136/vzj2019.02.0021.
Zheng, W., Zeng, S., Bais, H., LaManna, J.M., Hussey, D.S., Jacobson, D.L., Jin, Y., 2018. Plant Growth-Promoting Rhizobacteria (PGPR) Reduce Evaporation and Increase Soil Water Retention. Water Resour. Res. 54 (5), 3673–3687. https://doi.org/10.1029/2018WR022656.
Zickenrott, I.-M., Woche, S.K., Bachmann, J., Ahmed, M.A., Vetterlein, D., 2016. An efficient method for the collection of root mucilage from different plant species-A case study on the effect of mucilage on soil water repellency. J. Plant Nutr. Soil Sci. 179 (2), 294–302. https://doi.org/10.1002/jpln.201500511.